Physico-chemical characterization and immunomodulatory activity of bifidobacterium longum exopolysaccharide polyelectrolyte multilayer coatings

Romain Bagnol, Claudia Siverino, Vincent Barnier, Liam O'mahony, Dirk W. Grijpma, David Eglin, T. Fintan Moriarty

Target journal: ACS Biomacromolecules

Title: Physico-chemical characterization and immunomodulatory activity of bifidobacterium longum exopolysaccharide polyelectrolyte multilayer coatings

Authors: Romain Bagnol[1,2], Claudia Siverino[1], Vincent Barnier[3], Liam O'Mahony[4], Dirk Grijpma[2], David Eglin[2,5], T. Fintan Moriarty[1]

Affiliations:
[1] AO Research Institute Davos, Davos, Switzerland,
[2] Technical Medical Centre, Department of Advanced Organ Engineering and Therapeutics, Faculty of Science and Technology, University of Twente, Drienerlolaan 5, 7522 NB Enschede, the Netherlands,
[3] Mines Saint-Etienne, CNRS, UMR 5307 LGF, Centre SMS, F-42023 Saint-Etienne, France,
[4] Departments of Medicine and Microbiology, APC Microbiome Ireland, University College Cork, Cork, Ireland,
[5] Mines Saint-Étienne, Univ Lyon, Univ Jean Monnet, INSERM, U1059 Sainbiose, Saint-Étienne F - 42023 France.

Keywords: *Bifidobacterium Longum*, polyelectrolyte, exopolysaccharide.

Abstract (150 words)

Immunoregulatory polysaccharides from probiotic bacteria have potential for application in biomedical engineering. Here, a negatively charged exopolysaccharide from *Bifidobacterium longum* with confirmed immunoregulatory activity (EPS624), is applied in multilayered polyelectrolyte coatings with positively charged chitosan.

EPS624 and coatings (1, 5, 10 layers, and alginate-substituted coatings) were characterized by zeta potential, Dynamic light scattering, Size Exclusion Chromatography, Scanning electron microscopy, and Atomic force microscopy. Peripheral blood mononuclear cells (hPBMCs) and fibroblasts were exposed for 1, 3, 7 and 10 days with cytokine secretion, viability and cell morphology as observations.

The coatings showed an increased rugosity and exponential growth mode with increasing layers. A dose/layer dependent IL-10 response was observed in hPBMCs, which was greater than EPS624 in solution, and was stable over 7 days. Fibroblast culture revealed no toxicity or metabolic change.

The EPS624 polyelectrolyte coatings are cytocompatible, have immunoregulatory properties and may be suitable for further investigation in biomedical engineering.

Introduction:

Bacterial exopolysaccharides (EPS) are polymeric sugars produced by bacteria that are either located external to, or attached to, its outer membrane. EPS serve many functions for bacteria including protection from environmental stressors [1], as a reservoir of water or nutrition [2], and, in medically important bacteria, as an aid to pathogenicity [3]. *Bifidobacterium longum* is a Gram-positive commensal bacterium present in the human gut. *B. longum* is known to produce EPS, which are believed to aid adhesion to the intestinal epithelium and survival in the presence of low pH (in the stomach), bile salts and pancreatic enzymes, as well as being a mediator molecule in the dialogue between the bacterium and the intestinal mucosa [4].

Bacterial exopolysaccharides in general display good biocompatibility, biodegradability and non-toxicity, making them suitable candidates for biomedical engineering. The most widely used bacterial EPS in biomedical applications include the use of cellulose [5] due to its excellent mechanical properties and high water retention capabilities; alginate [6] due to the facile crosslinking potential; and xanthan gum due to its excellent water solubility, biocompatibility, immune inertness and positive viscoelastic properties [7]. Various bacterial EPS have been used for bone regeneration [8], rheological enhancement, drug delivery and tissue engineering [9] as well as in wound healing [5] and osteoarthritis [7].

In many cases, the EPS may serve as a rather inert, biocompatible component in a composite biomaterial that may be loaded with other active agents. However, a small number of EPS structures have been shown to retain independent biological activity. For example, EPS from a *Bacillus circulans* [10] and a *Bacillus Amyloliquefaciens* [11], showed general and COX-2 specific anti-inflammatory properties, which were hypothesized to be related to cell membrane stabilization, which was tested for red blood cells in vitro, and proteinase inhibition [10] and nitric oxide inhibition [11]. Another EPS from a *Lactobacillus paraplantarum* has been shown to reduce inflammatory cytokines and hyperalgesia in rats, linked to increased IL-10 and IL-6 induction [12]. Another polysaccharide of interest is the EPS624 from *Bifidobacterium Longum subsp. Longum 35624*, which has confirmed immunoregulatory properties. EPS624 has been shown to increase IL-10 secretion and regulatory T cell recruitment in a number of animal models or allergic airway diseases [13-15]. The IL-10 induction was shown to follow a TLR-2 dependent pathway [16]. More recently it was shown that EPS624 could prevent osteoclast maturation under homeostatic and tumor necrosis factor alpha (TNF-α) induced inflammatory conditions [16], suggesting it may have bone protective effects. However, when the EPS-producing *Bifidobacterium 35624* strain was administrated orally in mice, it was only partially effective at preventing ovariectomy induced bone loss, suggesting limitations of oral administration of EPS624 to achieve biological activity in the bone. To overcome this potential loss in activity due to oral ingestion, local application of EPS624 directly to the bone could potentially be a beneficial approach to improve bone-targeted activity.

Polyelectrolyte coatings are an effective method to combine positively and negatively charged polymers, creating multilayered coatings that may easily be loaded with hydrophilic molecules [17]. Since they do not require reactive molecular bonds, polyelectrolyte coatings retain the biological activity of their constituent components to a larger degree than chemical immobilization methods [18]. Furthermore, by adjusting the number of layers, the amount of material on the surface and the subsequent release kinetics may be influenced. Polyelectrolyte coatings from natural polymers have been used for a variety

of applications including blood-compatible chitosan/heparin coatings to reduce coagulation at the implant surface due to their cytophilic and anticoagulant properties [19], increased biocompatibility for orthopedic and dental implants, when using chitosan and heparin [20], anti-microbial activity [21, 22], for example in a hyaluronic acid/polyarginine system [22], and drug delivery such as loading tamoxifen, which is an anti-cancer drug, into chitosan/alginate films . A polyarginine/hyaluronic acid polyelectrolyte system also reduced the innate immune response in a two-step granuloma formation model [23].

Polyelectrolyte coatings composed of immunoregulatory bacterial EPS have not been previously described. Therefore, the aim of this study was to prepare and characterize immunomodulatory polyelectrolyte coatings using the negatively charged EPS624 with positively charged chitosan. In particular, we characterize the physico-chemical properties of the polymers used in the polyelectrolyte coating process, as well as the polyelectrolyte coatings surfaces themselves by scanning electron microscopy and atomic force microscopy. In addition, we investigated the cytokine response of human PBMCs and fibroblast cytotoxicity when exposed to solubilized EPS624 and polyelectrolyte coatings containing EPS624. Our hypothesis is that EPS624 polyelectrolyte coatings can be constructed and retain immunoregulatory activity, measured by induction of IL-10 secretion from exposed cells.

Materials and methods:

EPS624 production and purification

Bacterial culture

Bifidobacterium Longum subsp. Longum 35624 (NCIMB 41003 (35624TM)) was acquired from NCIMB Ltd (Aberdeen, UK) and stored in 20% glycerol stocks at -80°C.

Production and purification of EPS624 was performed based on a previously described protocol [13, 24]. Briefly, the bacteria were first grown in de Man Rogosa and Sharpe Medium (MRS Broth; Sigma; St. Louis, MO, USA) supplemented with 0.05% L-cysteine-HCl (L-Cysteine-HCl, Sigma; St. Louis, MO, USA) and 3% glucose (D-Glucose, Sigma; St. Louis, MO, USA), at 37°C under anaerobic conditions (GasPak EZ Anaerobe Container System, Becton Dickinson, Franklin Lakes, USA) for 72h. The culture was then transferred to modified MRS agar (MRSA) plates. MRSA (per liter) was composed of: Bacteriological Agar 15g, 10g peptone from casein, 2.5g yeast extract, 3g tryptose, 3g K_2HPO_4, 3g KH_2PO_4, 3g Ammonium Citrate Tribasic, 0.2g sodium pyruvate, 1mL Tween 80, 0.575g $MgSO_4*7H_2O$, 0.12g $MnSO_4*4H_2O$, 0.034g $FeSO_4*7H_2O$ (purchased from Sigma; St. Louis, MO, USA) originally inspired from this patent. Cultures were grown under anaerobic conditions at 37°C for 3-5 days.

EPS purification

Bacterial colonies were collected using a cell scraper and resuspended in phosphate buffered saline (PBS; Sigma; St. Louis, MO, USA) + 1 µg/ml RibonucleaseA (Sigma; St. Louis, MO, USA) + 5 µg/ml Deoxyribonuclease I (Sigma; St. Louis, MO, USA) in sterile 50mL tubes. The tubes were shaken manually to resuspend the EPS, and then agitated for 2h on a shaking plate at 4°C. The bacteria were then removed by centrifuging the tubes at 20'000g for 30min at 4°C, and the supernatant filtered using 0.45 µm filters (TPP, Trasadingen, Switzerland).

The NaCl concentration of the EPS-containing supernatant was adjusted to 0.45M using saturated NaCl solution. The EPS was then precipitated by addition of 3 times its volume of 100% ethanol at 4°C under gentle manual stirring for 30s, before being stored for 2h at 4°C. The precipitate was then collected and resuspended in MilliQ™ water. The resuspended liquid was transferred in a 12-14 kDa dialysis membrane (Thermo Scientific, Waltham, Massachusetts, USA) and dialyzed for 3 days in MilliQ™ water at 4°C on an agitating plate, with 3 water changes per day. The dialyzed liquid was then purified by passing twice through reverse phase column chromatography, using SPE C18 columns Chromabond (CarlRoth; Karlsruhe, Germany) with a HyperSep-96TM vacuum manifold (Thermo Scientific, Waltham, Massachusetts, USA). Finally, the solution was filtered through 0.45um filters before being freeze dried over 4 days using a Christ Alpha2-4LD Plus (Martin Christ, Osterode am Harz, Germany). Dried EPS powders were stored at -80°C.

Polyelectrolyte coating

Polyelectrolyte coatings were composed from the EPS624 prepared as described above, chitosan with a 75-85% degree of deacetylation and an average molecular weight (Mw) between 190.000 and 310.000 Da (Sigma; St. Louis, MO, USA) and alginic acid (Acros Organic; Geel, Belgium). The coating substrates were 15mm diameter glass cover-slip disks (Biosystems; Muttenz, Switzerland). Glass disk holders were printed with commercial PLA (DIM3NSIONS GmbH; Aesch; Switzerland) on an Ultimaker 3 machine (Ultimaker; Utrecht; Netherlands). The coating protocol is shown in Fig. 1. MilliQ™ water was used for all solutions. The pH of the polyelectrolyte and rinsing solutions were adjusted using acetic acid and sodium hydroxide as appropriate. First, the glass disks were cleaned in 10mM sodium dodecyl sulfate (SDS), then 0.1M hydrochloric acid, then MilliQ™ water. For both EPS624 and chitosan polyelectrolyte baths, the concentration was 1mg/mL at pH 5 in MilliQ™, and the rinsing baths were MilliQ™ at pH 5. For control coatings (with alginate instead of EPS624), the alginate polyelectrolyte bath was 1mg/mL, pH 3 in MilliQ™, and the two following rinsing baths were MilliQ™ at pH 3. The cycle of dipping and rinsing was repeated 1, 5 or 10 times. At the end of the process the discs were rinsed in MilliQ™ water and dried at room temperature. The coating groups prepared were: uncoated glass disks, glass disks with 1, 5 and 10 layers of chitosan and EPS624 (1, 5 and 10) and finally glass disks with 10 layers of chitosan and alginate (10A). Specifically for the atomic force microscopy measurements, we included more chitosan/EPS624 coatings with different numbers of double layers being 1, 3, 5, 8, 10, 13, 15, 18 and 20.

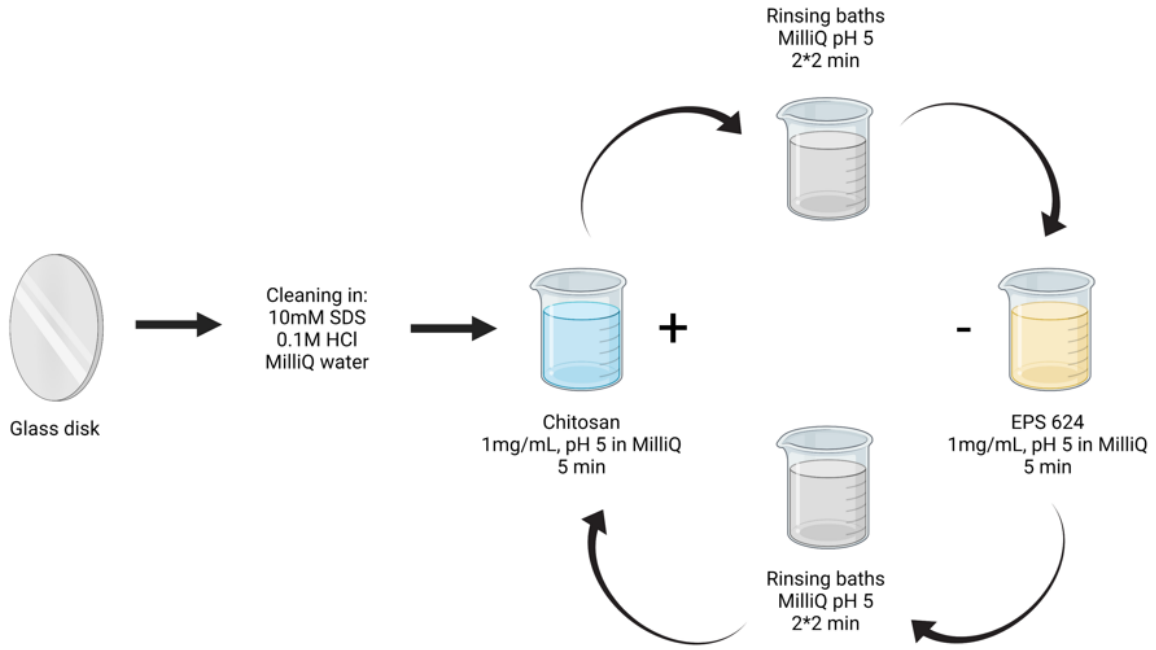

Figure 1: Scheme of the glass disk cleaning process and chitosan/EPS624 polyelectrolyte coating preparation process. Image prepared using Biorender®.

Characterization of EPS624

Titration Curve

Titration curves were made for 1mL of EPS624 by using hydrochloric acid and sodium hydroxide to control the pH of the solutions from 2.2 to 12.0.

Size Exclusion Chromatography (SEC)

The molecular characterization of EPS624 and chitosan was performed using a multi-detector size exclusion chromatography system. After solubilization, each sample was filtered through 0.45 µm nylon filters. The multi-detector SEC system used two on-line detectors: 1) multi-angle laser light scattering (MALS); 2) differential refractometer (DRI) as concentration detector. The molecular characterization allowed the determination of average molecular weights Mn, Mw and Mz, molecular weight distributions (MWD), macromolecule size and conformation. The MWD of EPS624 samples was obtained by a modular SEC system consisting of an Alliance 2695 separation module from Waters (Milford, Massachusetts, USA) equipped with two on-line detectors: i) MALS Dawn DSP-F photometer (Wyatt; Santa Barbara, California, USA); ii) 2414 differential refractometer (DRI) (Waters, USA) as concentration detector. Setup of the multi-detector SEC system was serial in the following order: Alliance-MALS-DRI.MALS detector uses a vertically polarized He-Ne laser, λ=632.8 nm, and simultaneously measures the intensity of the scattered light at 18 fixed angular locations ranging in the aqueous solvent from 14.5° to 158.3°. MALS detector coupled to a concentration detector allows to obtain the true molecular weight M and the size, i.e., the root mean square radius <s2>½in short to hereafter denoted as radius of gyration Rg, of each fraction of the eluting polymer.

Characterization of polyelectrolyte solutions

Zeta Potential

A Zetasizer Nano S series (Malvern Panalytical, Malvern, UK) was used to measure the zeta potential of the polysaccharides. Medium MW chitosan (Sigma; St. Louis, MO, USA) was dissolved in MilliQ™ water with 0.001M NaCl and 0.025M acetic acid at a concentration of 1mg/mL. Alginate (Acros Organic; Geel, Belgium) was dissolved at concentration of 1mg/mL in MilliQ™ water with 0.001M NaCl. EPS624 was dissolved at a concentration of 1mg/mL in 0.001M NaCl in MilliQ™ water. The pH of the solutions was adjusted to the desired values using acetic acid and sodium hydroxide. The measurements were made using a folded capillary zeta cell (Malvern Panalytical; Malvern, United-Kingdom) and were repeated 3 times for each group.

Dynamic light scattering (Rg)

A Zetasizer Nano S series (Malvern Panalytical; Malvern, United-Kingdom) was used for dynamic light scattering measurements to determine the average particle diameter of the polymeric chains of EPS624, alginate and chitosan in solution. Medium MW chitosan was dissolved in MilliQ™ water and 0.025M acetic acid at a concentration of 1mg/mL. Alginate was dissolved at concentration of 1mg/mL in MilliQ™ water. EPS624 was dissolved at a concentration of 1mg/mL in MilliQ™ water. The solutions were then diluted to 0.1mg/mL and 0.01mg/mL using the same specific individual dissolving solutions described above. For chitosan, the pH was adjusted to 5 using sodium hydroxide. The measurements were made using square polystyrene cuvettes (Malvern Panalytical; Malvern, United-Kingdom). Three different samples were used for each group.

Dry polyelectrolyte characterization

Scanning electron microscopy (SEM)

Scanning Electron microscope observations were conducted using a field emission Hitachi S-4700 II microscope (Hitachi Ltd, Tokyo, Japan) and a Quartz PCI image management system. After coating preparation on glass disks, the coatings were left to dry at room temperature, without any ethanol dehydration. The samples were sputter coated using gold palladium with a BAL-TEC MED 020 sputter coater connected to a BALTEC MCS 010 and a BAL-TEC QSG 060 (BAL-TEC AG, FL). Micrographs were taken with a working distance of 12mm, an accelerating voltage of 3.0 kV and a current of 40 µA.

Atomic Force Microscopy (AFM)

Topography, roughness, and thickness of the polyelectrolyte films were characterized by atomic force microscopy using a JPK Nanowizard® 3 instrument.

To determine the thickness of polyelectrolyte coatings, we used the ability of AFM to perform nanoscratching [25]. Taking advantage of that method was only possible due to the high differences in hardness between the soft polyelectrolyte films and the much harder glass disks they were deposited on. This methodology is illustrated in Fig. 2. Grooves were created by scanning 0.4x3 μm^2 areas using a TipsNano DRP-IN-C diamond coated silicon cantilever with single crystal diamond tip having 25 nm curvature radius. The cantilever sensitivity (34 nm/V) was calibrated by doing a force curve on a sapphire sample while the spring constant (198 N/m) was estimated using the thermal noise method [26]. Nano-scratching were carried out in contact mode at 10 Hz line scanning rate and using 400 nN applied force setpoint. These values were chosen in order to minimize the lips at the border of grooves as can be

seen in the Fig. 2A and to avoid damaging the substrate which was inspected after nano-scratching a glass disk reference sample. For each polyelectrolyte film, two grooves were performed: the first one consists of 20 scans and the second 40 scans. Just after grooving the polyelectrolyte film, the surface is imaged with the same cantilever using the Quantitative Imaging (QI) multiparametric mode developed by JPK Instruments which consists of high-speed acquisition of force-distance curve at each pixel image as illustrated in Fig. 2C. From the extent force curves, for each image pixel, one can extract the contact point ie. the height at which the cantilever just starts to touch the surface along with the slope in the repulsive part characterizing the material elasticity as can be shown respectively in the Fig. 2C and 2D. In order to estimate the polyelectrolyte film thickness, this one must be completely removed from the grooves by nano-scratching. This point is first validated by checking that the measured slope of extent force curve at these locations corresponds to the one measured (200 N/m) on the glass reference sample as illustrated in the Fig. 2D showing the height and slope profiles extracted from the Fig. 2A and 2B. The removing of the film is also confirmed by checking that the depth of the groove with 20 scans (the left one in the Fig. 2A) is equivalent to the one measure with twice the number of scans (the right one in the Fig. 2A). The film thickness is afterwards evaluated from the contact point height map subtracting the mean height value of the film measured on areas at each sides of the grooves from the mean height measured in the grooves as illustrated in the Fig. 2A. This measurement was carried out after a preliminary linear background plane correction of the contact point height map.

Morphologies of the polyelectrolyte films were characterized using a biosphere B20-NCH cantilever with resonance frequency of 330 kHz and spring constant of 40 N/m operated in dynamic intermittent contact mode. The cantilever had a spherical tip with 20 nm diameter. Small topographic features of the films were examined scanning 1x1 μm^2 areas with 512x512 pixel rate.

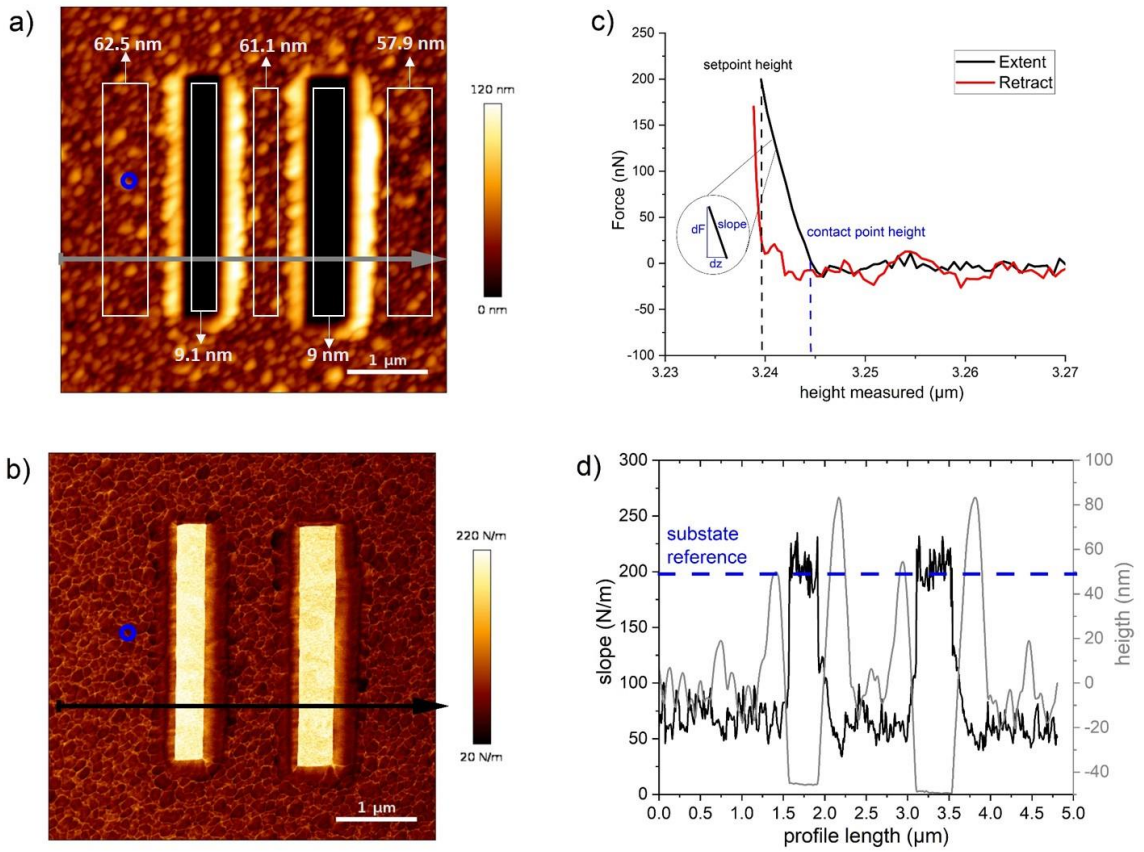

*Figure 2: Protocol used to evaluate the thickness of polyelectrolyte films by nano-scratching with an atomic force microscope. The example is taken for the polyelectrolyte film consisting of 15 deposited monolayers. Two grooves were machined by scanning 0.3*4µm^2 areas using a cantilever with single crystal diamond tip. The groove on the left in figure A) and B) corresponds to 20 consecutive scans while the one on the right corresponds to 40 scans. A) and B) represent the contact point height and slope mapping of force curves obtained after nano-scratching using the JPK Instrument Quantitative Imaging mode. An example of such force-distance curve corresponding to the blue circle location in figures A) and B) is presented in figure C) showing how slope and contact point height values are determined. Profiles of these two parameters corresponding to the grey and black arrows are presented in the figure D) where the blue dotted line corresponds to the value of force curve slope measured on a glass reference sample. The film thickness is evaluated by subtracting the mean height values obtained measured on polyelectrolyte film areas with the mean heights obtained in the two nano-scratched grooves. These areas are represented by white squares in the figure A).*

Biological assays

Viability of human fibroblasts exposed to polyelectrolyte coatings and EPS624 in solution

Telomerase-immortalized human foreskin fibroblasts (hTERT-BJ1) were used to test the biocompatibility of the chitosan/EPS624 and chitosan/alginate coated cover slips. hTERT-BJ1 were purchased from Clontech (USA) and were routinely cultured as previously described [27]. Briefly, hTERT-BJ1 were cultivated in alpha- Minimum Essential Medium (α-MEM) (Gibco™, ThermoFisher Scientific, USA) supplemented with 10 % fetal bovine serum (Corning, USA) with the addition of 100 µg/mL streptomycin (Gibco™, ThermoFisher Scientific, USA), 100 U/mL penicillin (Gibco™, ThermoFisher Scientific, USA) at 37 °C in a humidified 5% CO_2 atmosphere. Polyelectrolyte coated cover slips were

first placed in a 24-well plate and afterwards $5x10^3$ cells per well were seeded on top of the cover slip. The conditions tested included: 1, 5 and 10 layers of chitosan/EPS624, as well as 10 layers of chitosan/alginate (10A). Non-coated cover slips were used as positive control. In addition, cells were exposed to EPS624 dissolved in media at 1, 10 and 100 µg/ml. Cells were seeded in the well and the EPS624 solutions were applied the following day. As positive control, cells were grown in complete medium (α-MEM, 10% FBS and 1% P/S) without any EPS or coated cover slip. Cells treated with dimethyl sulfoxide (DMSO, Sigma-Aldrich, USA) were used as negative control.

To determine cell viability, CellTiter-Blue® (Promega, USA) was used at day 1, 3, 7 and 10 following the manufacturer's instructions. Cell viability (calculated in %) was determined as the fluorescence ratio between cells grown on EPS624 coated cover slips and non-coated cover slips for the coating assay, or cells exposed to the different concentrations of EPS624 and the positive control for the EPS624 dissolution in media assay. At each time point, cells were detached from the single well/coverslip and counted using an automatic cell counting device fluidlabR300 (Anvajo, Dresden, Germany). The average values and standard deviations were calculated from 3 replicates.

Human peripheral blood mononuclear cells (hPBMC) isolation from buffy coat

The hPBMCs used for the *in vitro* experiments were isolated from buffy coats provided by the Regional Blood Donation Service SRK Graübunden (Chur, Switzerland). The blood was diluted in PBS and carefully added to histopaque solution (Sigma; St. Louis, MO, USA) before being centrifuged at 800 rcf for 30min. The cell pellet was taken from the solution using a Pasteur pipette, resuspended in Roswell Park Memorial Institute (RPMI) media (RPMI Medium 1640, Gibco™, ThermoFisher Scientific, USA) and then centrifuged 10 min at 300 rcf and room temperature. The supernatant was removed, fresh media was added and the cells were centrifuged at 300 rpm for 10 min. After supernatant removal and dilution to the appropriate concentration, the cells were stored in a 50% RPMI, 40% FBS (Corning, USA), 10% DMSO solution, at $5*10^6$ cells/mL in liquid nitrogen. All experiments, except the final TNF-α ELISA, were performed using the same buffy coat. A second buffy coat, from a second donor, was required for the final experiment.

hPBMC culture and exposure to polyelectrolyte coatings/EPS624 in solution

hPBMCs were thawed from liquid nitrogen then cultured in RPMI media + 10%FBS (Corning) + 1% P/S for 24h at 37°C before being counted and diluted to a concentration of 500.000 cells/mL in RPMI + 10% FBS + 1% P/S for all experiments.

For experiments with EPS624 in solution the cells were cultured in 96 well plates, using 250 µL of media per well and EPS624 concentrations of 1, 10 and 100 µg/mL. For experiments with EPS624 polyelectrolyte coatings, the coated glass disks were first deposited at the bottom of 24 well plates and then 1mL of the RPMI media containing cells was added on top of each well.

In all cases, the cells were incubated for 24h at 37°C, after which the media in each well was centrifuged for 5 min at 350rcf. The supernatants were then collected in Eppendorf tubes and stored at -20°C. The experiment was repeated 4 times in total, with n=2 to 3 for each condition per assay.

Coating stability assay

Each disk was immersed in 5mL of sterile PBS in a sterile glass vial. The glass vials were placed in a 37°C incubator with 100 rpm agitation for 1, 3 or 7 days to allow release of EPS624 into the solution. At the end of the immersion period, each disk was rinsed in MilliQ™ water and dried at room temperature. The uncoated glass control group with no PBS immersion was also rinsed in MilliQ™ water and dried at room temperature. The disks were later used for the PBMCs experiments as described previously. The groups tested included chitosan/EPS624 coatings containing 1, 5 and 10 layers of each polymer, with all groups tested after 0, 1, 3 and 7 days immersion.

Cytokine measurements

Secreted Interleukin (IL-10) and Tumor Necrosis Factor (TNF-α) were measured in supernatants of the hPBMCs cultures using a human IL-10 Duoset ELISA (reference DY217B) and a human TNF-α Duoset ELISA (reference DY210) from R&D Systems (R&D Systems, Minneapolis, USA). A wider range of secreted pro and anti-inflammatory cytokines were measured using A U-PLEX T cell combo (hu) sector multikit (reference K15093, Mesoscale, RockVille, USA), that included the following markers: TNF-α, IFN-y, GM-CSF, MIP-3α, IL-2, IL-4, IL-9, IL-10, IL-13, IL-17A, IL-17F, IL17E-25, IL-21 and IL-22.

Statistics

GraphPad Prism 9 was used for all statistical analyzes. ELISA IL-10, and U-plex T cell combo (hu) experiments were repeated 3 times, with N=2 to 3 per condition for each singular experiment and the datasets used for statistical analysis combine all individual values from each of the triplicate experiments. For all experiments, each group from each dataset was tested for normal distribution with the following tests: Anderson-Darling test, D'Agostino and Pearson test, Shapiro-Wilk test, Kolmogorov-Smirnov test. If one group from a dataset did not pass the normal distribution on one of these 4 tests, then the dataset was considered as not normally distributed. According to this criteria, all dataset were not normally distributed, so a non-parametric Dunn's multiple comparison test was used to determine statistical differences between the groups of each dataset. Statistical significance is displayed as follows: ns or an absence of sign for no statistical difference, * for $p<0.05$, ** for $p<0.01$, *** for $p<0.001$, **** for $p<0.0001$.

Results & Discussion

EPS624 characterization:

The titration curve of the EPS624 is shown in Fig. 3A. An equivalence point is observed at a pH of 6.73. Quantifying the pH at half the volume of equivalence, a pKa of 2.45 is obtained, indicating that the EPS624 fraction purified is a rather weak acid.

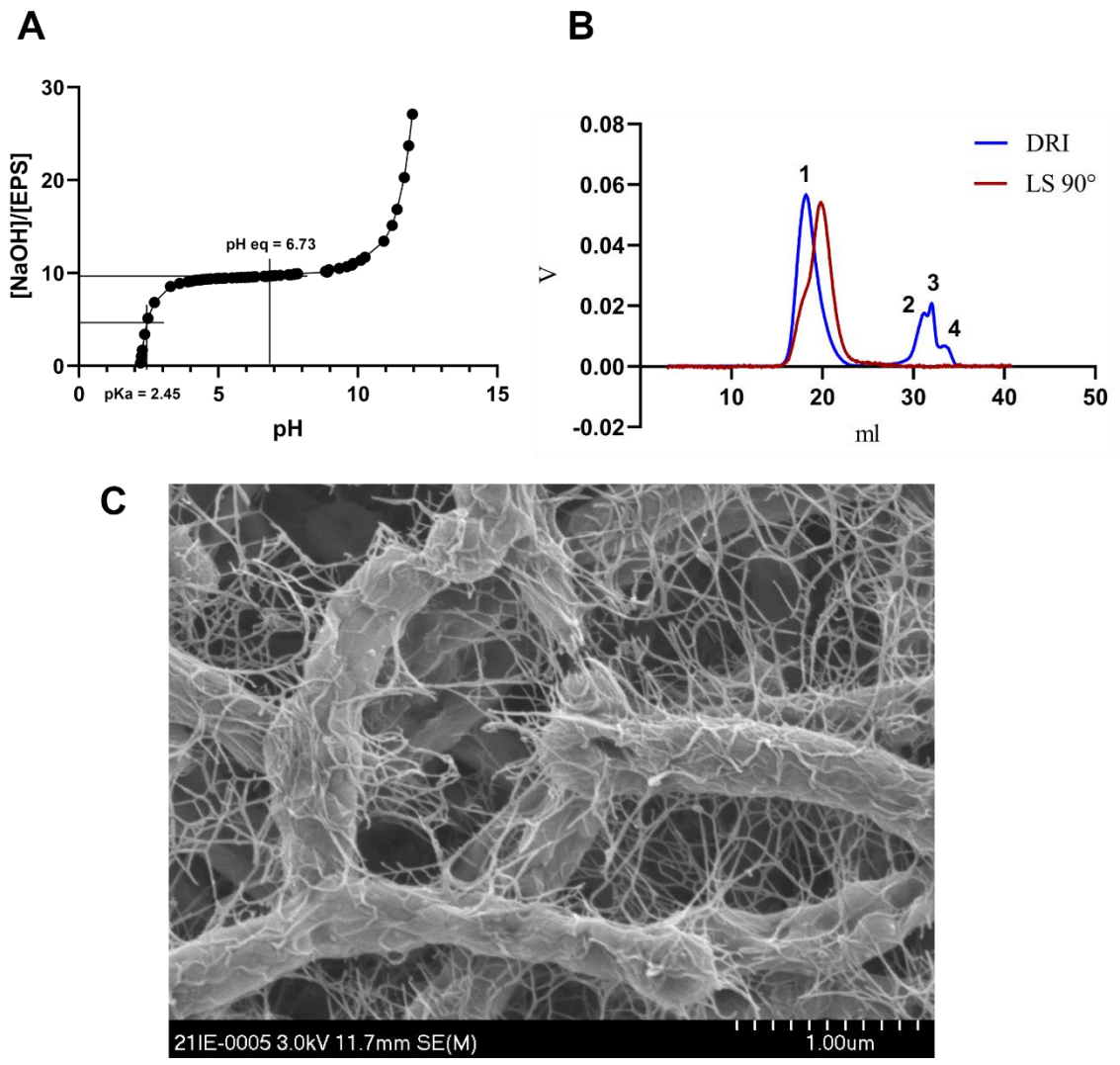

Figure 3: A: Titration curve of the EPS624 at 1mg/mL, with measured pKa.; B: Overlay of differential refractometer (DRI) and multi-angle laser light scattering (MALS) signals for EPS624 with peak being described in text; C: Scanning Electron Microscopy Image of Bifidobacterium Longum subsp. Longum 35624 and the associated EPS624 when grown on modified MRS agar.

The elution fractions of the EPS624 measured by DRI and MALS 90° detectors is shown in Fig. 3B, while the elution fraction of the chitosan is represented in Supplementary Figure 2. The EPS624 fraction measured by DRI is represented by one single peak 1, while the peaks 2, 3 and 4 represent impurities that can be attributed to remaining solvents, salts or proteins. List of calculated EPS624 molecular weights and gyration radiuses are reported Table 1. Equivalent data for chitosan is shown in Supplementary Table 1 and 2. A high molecular weight Mw of 639.9kg/mol is calculated in the range, 10 and 1000kg/mol, reported for other bacterial exopolysaccharides with a polydispersity of 1.9 [28].The MALS 90° (LS 90) elution curve shows two subpeaks. As EPS624 analysis by MALS has not been reported previously further investigations will be required to assess the presence of aggregation and conformational properties of the branched polysaccharide.

Table 1: Molecular weights and radii of gyration of EPS624 as determined by SEC, Rgn corresponding to the number average radius of gyration, Rgw to the mass average radius of gyration and Rgz to the Z-average radius of gyration.

Mn kg/mol	Mw kg/mol	Mz kg/mol	Mw/Mn	Mz/Mw	Recovered Mass (%)	Rgn nm	Rgw nm	Rgz nm	K nm	α
339.9	639.9	955.6	1.90	1.49	77.3	62.7	92.4	118.6	0.0306	0.599

Figure 2C is a Scanning Electron Microscopy image of the Bifidobacterium Longum subsp. Longum and associated EPS624 when grown on agar plates. The EPS624 can be seen attached to the bacterial cell wall and in between each cell, forming a "spider-net" like structure when in a dehydrated state.

Overall, the EPS624 production process yield a polysaccharide with a recovery mass above 75% with remnants attributed to solvent, salts and potentially others proteins. This is of high relevance as the impurities might affect the biological properties of the EPS624 and chitosan/EPS624 polyelectrolyte coatings. Potential sources of impurities are the MRS broth used to grow the bacteria, or other bacterial components from the Bifidobacterium released during the centrifugation step, due to the extreme speed used which very likely destroys bacterial cell membranes. These components could potentially bind to some of the EPS624 functional groups and therefore be present in the final product.

Characterization of solutions used in polyelectrolyte coatings:

The average polymer particle diameters in solution for alginate, chitosan and EPS624 are shown in Fig. 2B and Fig. 2C. At both 0.1 and 0.01mg/mL, alginate has the highest average particle diameter, followed by chitosan, with the lowest being EPS624. For alginate in particular, an increase in the particle diameter is observed as concentration increases, suggesting a degree of aggregation with increased concentration[30], which was not apparent for chitosan or EPS624. EPS624 displayed the lowest variation in diameter, suggesting a lower polydispersity of the average particle size, consistent with SEC results, compared with chitosan and alginate, which respectively showed a higher polydispersity or aggregation as concentration increases.

The Zeta Potential of the alginate, chitosan and EPS624 at different pH values is shown in Figure 4A. Both EPS624 and alginate have negative Zeta potential at all pH tested, while chitosan Zeta potential is positive in the same range. Alginate Zeta potential values are lower that EPS64 Zeta potential at all tested pH values. Overall, a decrease in Zeta Potential is observed with increased pH for all polymers, which is in accordance with published literature for chitosan [29]. The Zeta potential values indicates that EPS624 and chitosan in solution likely form polyelectrolyte complex like alginate and chitosan. Changes of polyelectrolyte baths pH and ionic strength influence solutions Zeta potential, increase colloidal stability and reduce the risk of aggregate formation prior to mixing. These also influence attractive forces between the positively charged and negatively charged polysaccharides when mixed and consequently the thicknesses and topographies of polyelectrolyte multilayer coatings as well as potential interactions will cells [32, 33]. A previously reported protocol for the formation of chitosan and hyaluronic acid polyelectrolyte multilayer coatings was replicated for the production of EPS624/chitosan polyelectrolyte

multilayer coatings [31].

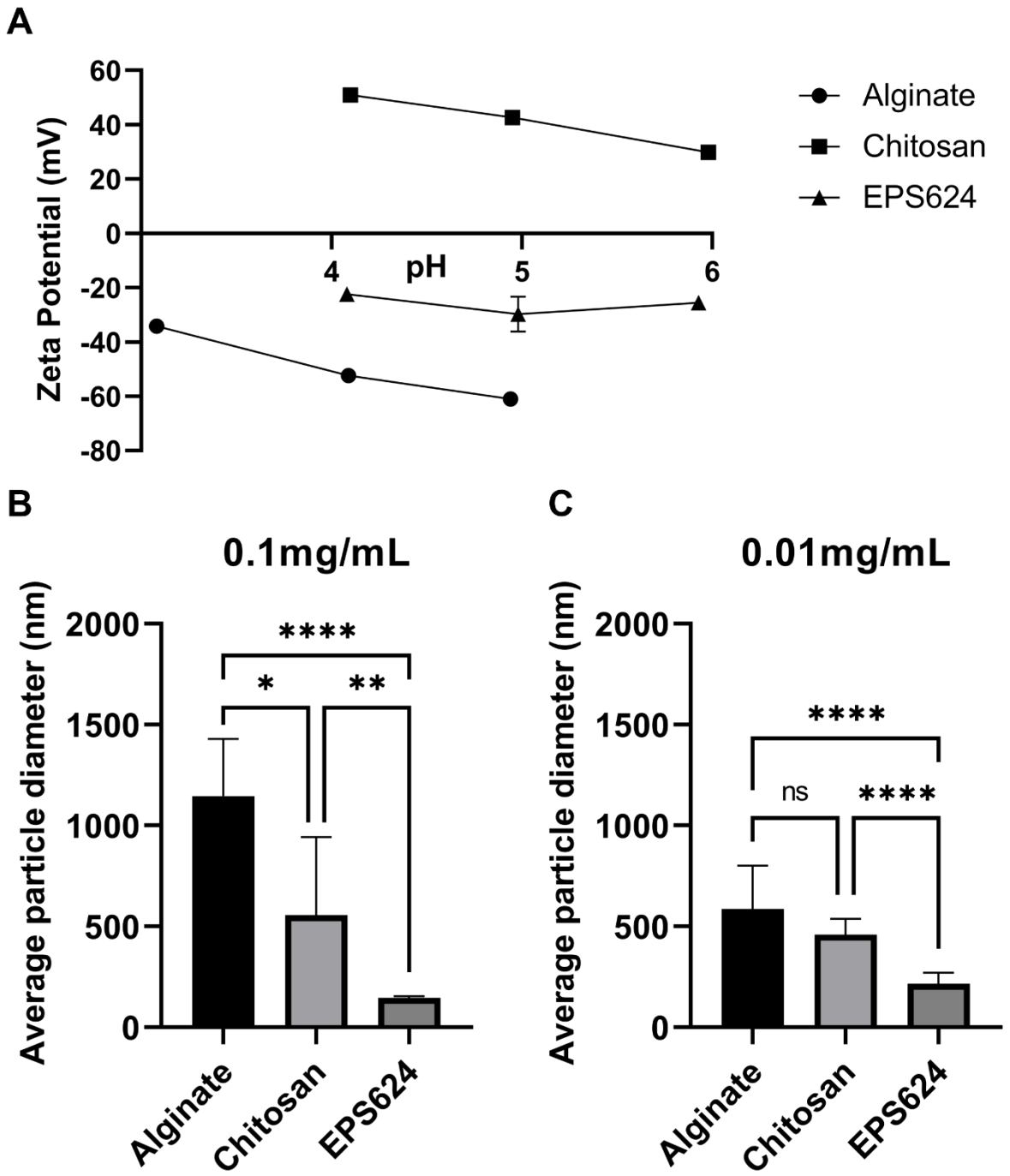

Figure 4: A: Evolution of measured Zeta potential of EPS624, alginate and chitosan at a concentration of 1mg/mL with pH; B: Average polymer particle diameter in solution at 0.1mg/mL as measured by dynamic light scattering; C: Average polymer particle diameter in solution at 0.01mg/mL as measured by dynamic light scattering

Dry EPS624/Chitosan polyelectrolyte coatings thickness, topography and mechanical properties

Atomic force microscopy

The formation and evolution of the polyelectrolyte coating with increasing number of layers was followed by AFM (Fig. 5A). The coating thickness follows an exponential growth in the range of layers explored up to 70 nm for 20 chitosan/EPS624 multilayer coating. The surface morphologies of polyelectrolyte

coatings consisting of 1, 5 and 13 double layers are shown in Fig. 5C D and E. The surface morphology of a monolayer predominantly exhibits a small structural feature reminiscent of phase-separated polymers with blisters of less than 50 nm. Theses blisters grow in size and number, and finally cover the entire surface-giving rise to a globular texture with objects of diameters up to 150 nm in the case of 13 double layers sample. The thickness exponential growth together with the globular objects of growing diameters are concurrent in supporting a mechanism of chitosan/EPS624 multilayers formation based on the diffusion through the film of one of the polysaccharide “in” and “out” during build-up has been described for polylysine/hyaluronan polyelectrolytes [34]. Meanwhile, the roughness values present a linear correlation with the number of layers (Fig. 5B). Since the nanoscale topographies affect cell behaviors [37], we might hypothesize that the number of layers could change cellular response not only based on the amount of material contained in the coating, but also in the topological and mechanical cues given to the cells [38].

Previous research has shown that the differences between dry and wet polyelectrolyte coating thicknesses are heavily dependent on the system used, with for example a thickness increase of only a few percent in a chitosan/chondroitin sulfate system but higher than 90 percent in a chitosan/hyaluronic acid system [35]. Measurements of the levels of hydration of polyelectrolyte coatings in situ also show large differences based on the system used, being for example 76% for poly(L-lysine)/Hyaluronic acid coatings, 63% for poly(L-lysine)/Chondroitin sulfate A coatings and 20% for poly(L-lysine)/Heparin coatings [36].

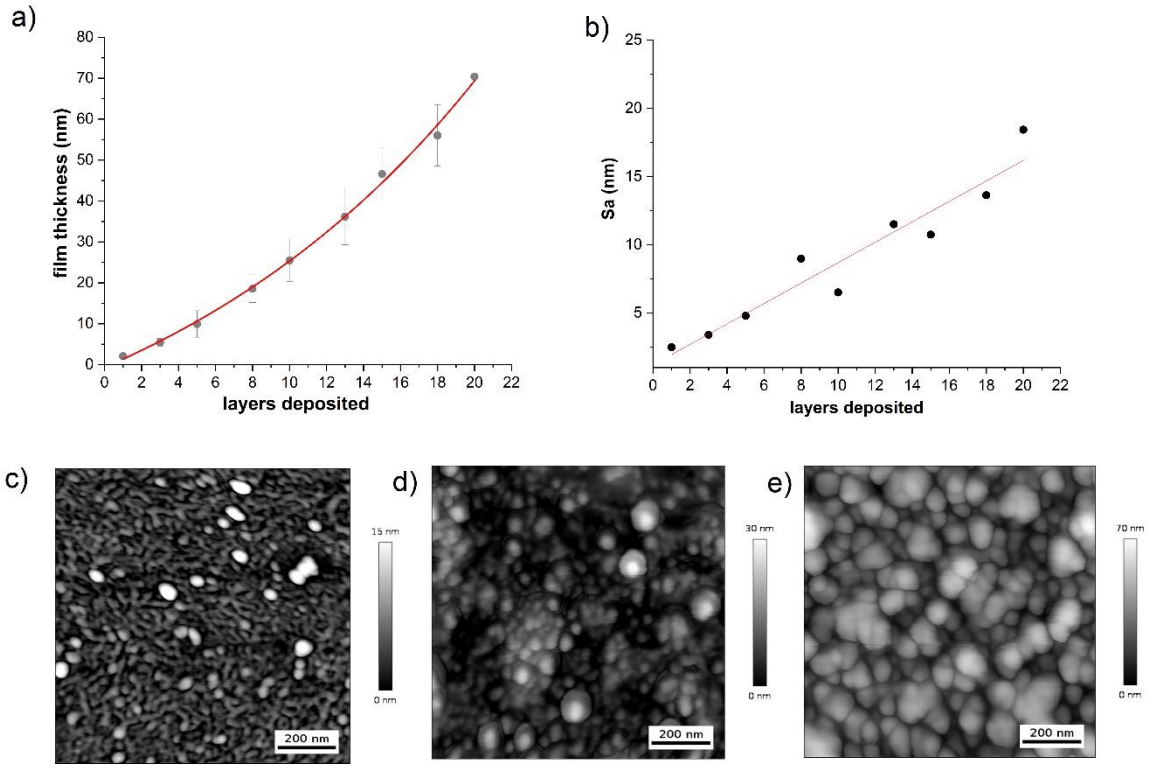

Figure 5 : A) evolution of polyelectrolyte film thickness determined by the nano-scractching method presented in the Fig. 2 and B) roughness (arithmetical mean height) in function of the number of layers deposited during the film elaboration protocol. The film structuring with the number of deposited layers is highlighted by intermittent contact AFM imaging in the figures C), D) and E) showing respectively the surface morphologies of 1, 5 and 13 monolayers deposited films.

Scanning Electron Microscopy (SEM)

Polyelectrolyte coatings observed by Scanning Electron Microscopy are shown in Fig. 6, with noticeable differences between the groups. The clean uncoated glass disc, used as substrate material for the coatings, shows a very smooth surface with no apparent rugosity or irregular topography. When looking at the chitosan/EPS624 groups, noticeable changes in topography are observed as the number of layers increases. In the 1 layer group, polysaccharide deposition on top of the glass surface is visible. While an overall smooth surface is observed, several deposits of presumptive polysaccharides, with width ranging from 30nm to 300nm, can be observed everywhere on the surface. As the number of layers increases to 5 and then 10, an increase in the overall rugosity of the surface as well as an increase in density of these particular deposits are seen. In comparison, the 10 layers alginate group shows an overall much smoother topography with fewer particular deposits. We hypothesized the presence of these particular deposits and change in rugosity were the results of the attachment of EPS624 or chitosan particles as the width of these particles were compatible with the particle diameter measured by dynamic light scattering (Figure 4B and 4C). However, we think this change in topography and rugosity is most likely due to the exponential growth of the coatings that was previously discussed in the atomic force microscopy section, as polyelectrolyte coatings with evolving topographies were already observed in other systems [32].

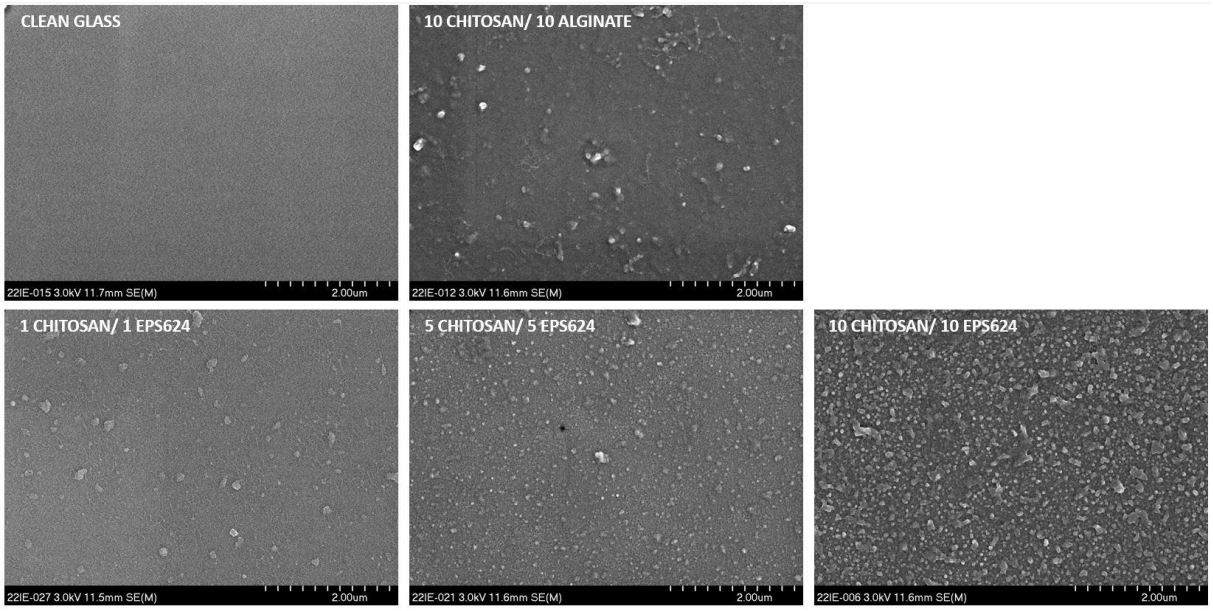

Figure 6: Images of EPS624/Chitosan and Alginate/Chitosan polyelectrolyte coatings by Scanning Electron Microscopy

Cell viability of human fibroblast after exposure to EPS624 and growth on polyelectrolyte coatings

The influence of EPS624 in solution on human fibroblast metabolic activity were tested after 1, 3, 7 and 10 days. Cells exposed to 1, 10 or 100 µg/ml of EPS624 show no changes in metabolic activity over 7 days with values comparable between these 3 conditions and the positive control (Figure 7 A). However, the cell count trended downwards with increasing EPS624 concentration at day 1 (Figure 7 B). On day 3, all the conditions are in the range of ~$6x10^4$ cells, while a net increase is measured at day 7 (~ $2.3x10^5$ cells). However, when normalizing the metabolic activity to the cell number, it appears as a general trend that a lower cell number corresponds with a higher metabolic activity (Supplementary Fig. 3A). This trend is higher for EPS 100 µg/ml and EPS 10 µg/ml compared to EPS 1 µg/ml and the positive control on day 1 and day 3. We can hypothesize that due to the attachment of an absolute lower number of cells, the lower cell density requires a higher need for proliferation before reaching confluency, which could lead to a higher individual cell metabolic rate. Another possibility is a direct effect on cell proliferation rate [39], as EPS-A28, another bacterial exopolysaccharide from Alteromonas PRIM-28 was shown to increase dermal fibroblasts proliferation by increasing cell activity during the S-phase cycle and expression of fibroblast Ki-67 proliferation marker [40].

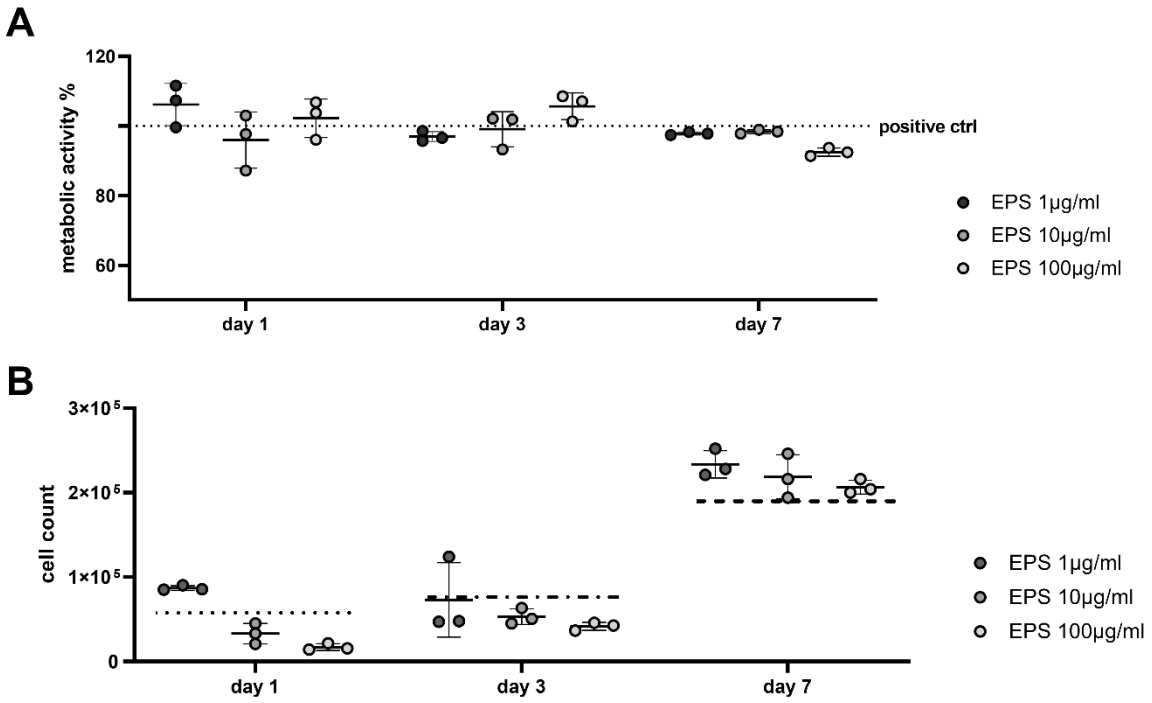

Figure 7: A: Human fibroblast hTERT-BJ1 exposed to EPS624 for 1, 3 and 7 days. **A.** Cell metabolic activity of hTERT-BJ1 exposed to 1, 10 or 100 µg/ml of EPS624 in complete medium (α-MEM, 10% FBS, 1% P/S). Cell metabolic activity is shown in % and was determined as the fluorescence ratio between cells exposed to EPS624 and positive control (cells in complete medium). Dashed line represents the positive control, 100 %. **B.** Cell count of hTERT-BJ1 exposed to 1, 10 or 100 µg/ml of EPS624 in complete medium (α-MEM, 10% FBS, 1% P/S). At every time point, cells were detached from the single well and counted. Dashed lines represent the mean of the positive controls at each time point.

The various EPS624/chitosan polyelectrolyte coated cover slips were also exposed to human fibroblast to evaluate cell attachment, proliferation, and metabolic activity over 10 days (Figure 8). While not significant, cell metabolic activity at day 1 and day 3 shows a trend of lower activity for 5 and 10 layers compared to 1 layer and to the positive control (Figure 8, A). For all days, we observe the chitosan/alginate coatings (10A) have the lowest metabolic activity out of all the groups. In contrast to observations in the case of the EPS624 in solution, the lower metabolic activity correlates with the lower cell number (Figure 8 B).

Additionally, cell attachment and proliferation on the polyelectrolyte coated cover slips appears strongly influenced by the number of chitosan/EPS624 layers when observed through microscopy (Supplementary. Fig. 1). The 5 layers and 10 layers groups induce a more aligned organization of the cells, compared with the more commonly observed random and more disperse cell attachment. The differences in cell attachment, proliferation and organization are most likely due to the evolving surface properties of the polyelectrolyte coatings as the number of layers increases. According to the Wenzel model, an increase in surface roughness can increase the hydrophobicity of hydrophobic surfaces, as well as increase the hydrophilicity of hydrophilic surfaces [41]. The hydrophilicity and hydrophobicity of a surface largely determines protein adsorption and protein denaturation, which in turn influence subsequent cell behavior [42]. Changes in roughness, that were observed by atomic force microscopy, have previously been shown to affect cell adsorption and migration [43], and it was observed that a moderately hydrophilic surface with a contact angle of around 70° led to the best fibroblast proliferation [44]. In addition, topographical structures, such as the presence of grooves and ridges can also influence protein adsorption and promote cells to align in the direction of the grooves and ridges [45]. As observed with the SEM and AFM data, we see an increase in surface roughness as the number of layers increases, and the AFM data shows an evolution of the topographic profile of the coatings as the number of layers increases. These two parameters could explain the initial difference in cell attachment, as well as the aligned orientation of the cells is the groups with more layers. Surface compliance is another element playing a role in cell behavior, with cells generally attaching and migrating more on stiffer/harder surfaces [46]. Due to the very thin nature of the coatings, we can hypothesize that the stiffness that the cell can "feel" would be higher for the coatings with lower numbers of layers, as the distance with the glass substrate is very small and it can probably still be felt, while this effect gets lower as the thickness of the polyelectrolyte coating increases, where the cell predominantly feel the properties of the polyelectrolyte coating. This could explain a lower attachment for groups with a higher number of coatings. A final potential reason for this observation is the changing of the surface charge of the coating as the number of layer increases. With the exponential growth of the coatings shown in Fig. 5A, we can hypothesize that higher amounts of EPS624 are present at the surface sensed by the cells, potentially changing the surface charges that can also influence protein adsorption and, therefore, cell behavior. While we initially see a lower adhesion for the 5 layers and 10 layers groups, the cells attach in a more aligned manner and are able to grow, and there is no difference in cell number and metabolic activity at day 10, showing all coatings are adequate surfaces for fibroblast growth.

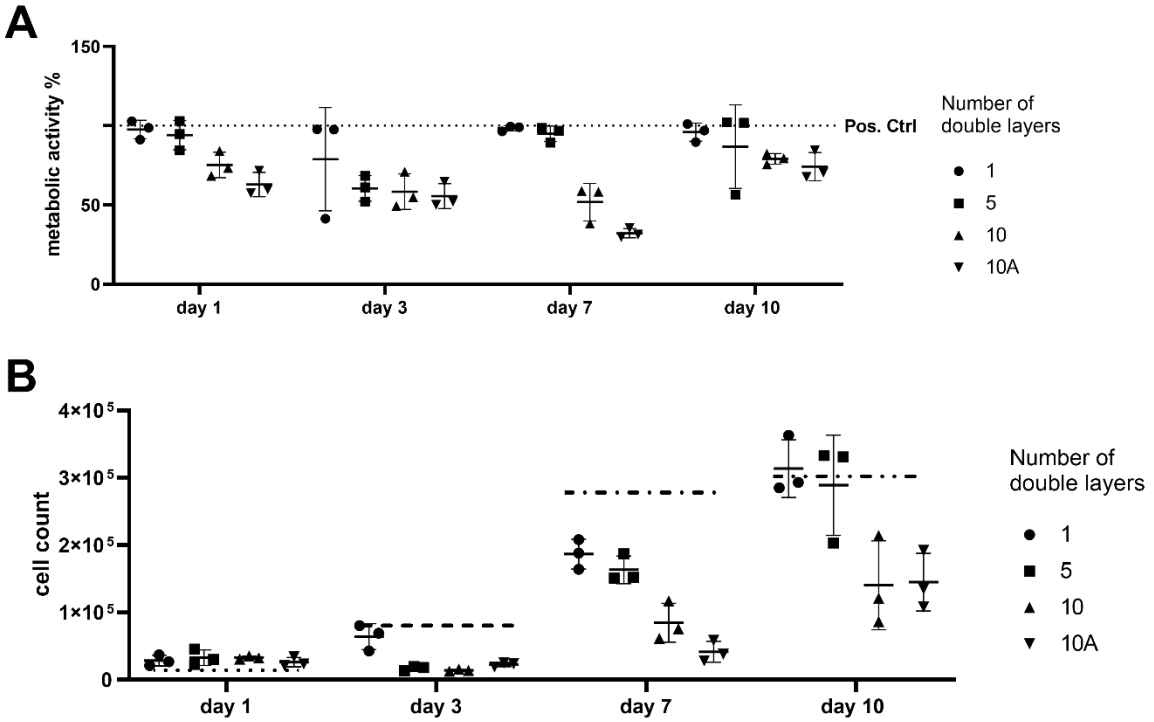

Figure 8: A: Human fibroblast hTERT-BJ1 *grown on EPS624 coated coverslips for 1, 3, 7 and 10 days.* **A.** Cell metabolic activity of hTERT-BJ1 grown on the different cover slips functionalized with either 1, 5 or 10 layers of EPS624 and chitosan (1, 5 and 10) or 10 layers of alginate and chitosan (10A). Cell metabolic activity is shown in % and was determined as the fluorescence ratio between cells grown on functionalized cover slip and positive control (cells on non-functionalized cover slips). Dashed line represents the positive control, 100 %. **B.** Cell count of hTERT-BJ1 grown on the different cover slips functionalized with either 1, 5 or 10 layers of EPS624 and chitosan (1, 5 and 10) and 10 layers of alginate and chitosan (10A). At every time point cells were detached from the single well and counted. Dashed lines represent the mean of the positive controls at each time point. The average values and standard deviations were calculated from 3 parallel samples.

Bacterial adhesion on polyelectrolyte coatings

Staphylococcus aureus adhesion to the polyelectrolyte coatings was assessed for 24h and 4 days, with methods and results shown in Supplementary Figure 4. Overall, the number of layers per coatings did not affect bacterial adhesion significantly, however the adhesion was increased in the coated cover slips compared to the uncoated cover slips. While the number of polyelectrolyte coatings layers affect fibroblast adhesion, it seems that *S. aureus* adhesion is not affected. Inactivated *L. casei* biofilms were shown to have anti-bacterial activity on methicillin resistant *S. aureus* in the literature, however it seems these effects were related to the presence of lactic acid and bacteriocin in the biofilm, and not the structure of the exopolysaccharide in contained [47].

IL-10 secretion by hPBMCs:

IL-10 secretion was previously shown to be specifically induced by EPS624 in monocyte derived dendritic cells [15] and osteoclasts precursor cells [16] and we investigated whether this IL-10 induction is also present in hPBMCs when EPS624 was incorporated into polyelectrolyte coatings.

IL-10 secretion by hPBMCs after exposure to EPS624, either dissolved in media or incorporated in polyelectrolyte coatings, is shown in Fig. 9A and Fig. 9B. When dissolved in media, a dose response effect is observed with increase of IL-10 secretion when exposed to increasing concentrations of EPS624 ($p<0.05$). The concentration levels inducing an IL-10 response are coherent with what was observed in osteoclast precursor cells where a concentration of 50µg/mL increased IL-10 secretion [16], while in monocyte derived dendritic cells, a trend for increased IL-10 secretion was observed up to 200 µg/mL concentrations [15]. However, failure to further increase IL-10 levels after increasing from 10µg/mL to100µg/mL suggests an upper threshold is reached beyond which higher IL-10 secretion is not achieved.

When looking at EPS624 incorporated in polyelectrolyte coating, a dose-dependent increase is also observed as the number of layers in the EPS624 coatings increases. However, the 5 and the 10 layers groups show no statistical difference suggesting a "saturation effect". The IL-10 response is of higher magnitude in the chitosan/EPS624 polyelectrolyte coatings compared to the EPS624 dissolved in media at 10ug/mL and 100ug/mL, however it does not reach statistical significance. One hypothesis for this higher secretion is that despite a low total amount of EPS624 in the coating, which was estimated in supplementary data and could theoretically lead to a maximal EPS624 concentration of 4.41ug/mL for the 10 layers groups, and lower concentrations for the other groups, its direct contact to the cells on the surface might lead to a higher exposure of the polymer to the cell receptors, therefore potentially increasing IL-10 expression.

Another interesting observation is the much lower IL-10 secretion in the 10 layers chitosan/alginate group compared to the 10 layers chitosan/EPS624 group ($p<0.01$). This finding confirms the specificity of the EPS624 for IL-10 secretion. Alginate is a well-known biomaterial with a good biocompatibility often used for wound dressing, however it does not have the specific IL-10 secretion activity of the EPS624. This property of EPS624 coatings may therefore, offer additional biologically advantageous properties compared with conventional equivalents.

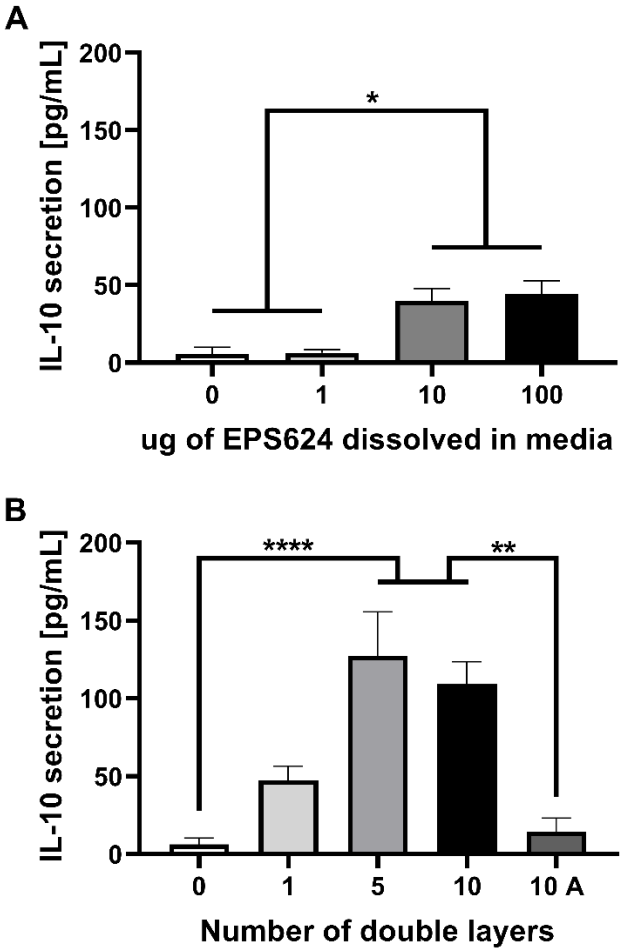

Figure 9: A: human peripheral blood mononuclear cell secretion of IL-10 when exposed to EPS624 dissolved in RPMI media for 24h, quantified by ELISA. Experiments were repeated 4 times with n=3 for each condition; B: human peripheral blood mononuclear cell secretion of IL-10 when exposed to EPS624/chitosan with different number of layers or alginate/chitosan with 10 layers (10A) polyelectrolyte coatings for 24h, quantified by ELISA. Experiments were repeated 4 times with n=2-3 for each condition, the total amount of sample N is between 10 and 12 for each group

Coating Stability:

To estimate the stability of the EPS624 coatings, they were stored in in PBS for 0, 1, 3 or 7 days and subsequently cultured with hPBMCs as represented in Figure 10. A reduction in IL-10 secretion was seen between the control groups (0 day) and the 1, 3 and 7 days groups, with often no statistically significant difference between day 1, 3 and 7. Higher secretions for the 5 and 10 layers groups compared to the 1 layer group are also observed.

The initial drop in IL-10 secretion between the control and the first day could be attributed to a fast release in the PBS of weakly bound polymer chains/particles during the first 24 hours. The subsequent constant IL-10 secretion thereafter suggests a relative resistance of the coating to degradation by hydrolysis. Another possibility for the main degradation mechanism of the coating is the dissolution of the polymer matrix rather than a scission of the polymer chains. This suggests that the coating could keep its activity for several days, and potentially longer. It can be hypothesized that with a higher number

of layers, a sufficient amount of EPS624 might be available to the cells for a longer time, potentially increasing the duration of biological activity. In vivo, oxidative reactive species can degrade polysaccharides which are actively transported by phagocytes [48]. Our in vitro approach does not account for active biological degradation and chemically induced degradation with slow kinetics, and could be an area for further characterization of these coatings to estimate in vivo activity profile.

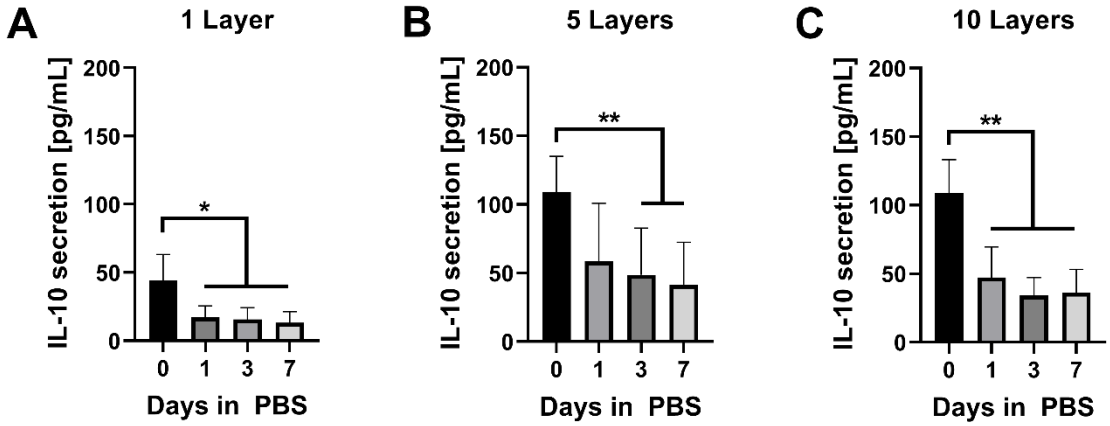

Figure 10: human peripheral blood mononuclear cells secretion of IL-10 when exposed for 24h to A: 1 layer, B: 5 layers, C: 10 layers of EPS624/chitosan polyelectrolyte coatings after being soaked in PBS for various lenghts of time, quantified by ELISA. Each graph combines the data of 4 different experiment with n=2-3 for each condition, the total amount of sample N is between 8 and 10 for each group

Pro and anti-inflammatory cytokine secretion in vitro:

Subsequently, a larger panel of cytokines were analyzed from the hPBMC supernatants to provide a broader perspective on potential immune responses to the EPS624 coatings. Negligible concentrations are measured for IL-2, IL-4, IL-9, IL-13, IL-17F, IL17E/25, IL-21 and IL-22. The results for these, and all other tested analytes can be found in the Supplementary Fig.5 and Fig.6. IL-10 secretion in Fig. 6A and Fig. 6B, shows very similar trends to the one observed for the ELISA-IL10 secretion. These results suggest an IL-10 specific response following exposure to EPS624. TNF-α was also quantified as it is an important cytokine. It is produced during an acute inflammation phase. Its concentrations remain high in a chronic inflammation, but are decreasing in a normal anti-inflammatory healing process mediated notably by an IL-10 secretion.

Dissolved in media, EPS624 induce a TNF-α dose dependent response for concentrations above 10mg/mL. On all coatings, higher TNF-α concentrations are measured in media for seeded and cultured hPBMCs (Fig. 11D). The high TNF-α secretion could be partially responsible for the IL-10 secretion measured. Interestingly, the 10 layers chitosan/alginate group induces a high TNF-α secretion indicating that EPS624 alone is not responsible for the observed increased. hPBMCs were then exposed to each of the polymeric reagents dissolved in media. Alginate shows low levels of TNF-α induction for all concentrations tested while chitosan shows a significant and strong dose dependent response (Supplementary Fig. 7). The chitosan effect on the TNF-α concentrations and pro or anti-inflammatory

response in vitro and in vivo have been reported elsewhere and are highly dependent on its molecular weight, preparation method, as well as the previous stimuli to which the cells were exposed [49,50,51]. EPS624 also shows a dose dependent TNF-α response caused either by endotoxin contamination, by the presence of residual proteins and bacterial products in the tested batch or by inherent EPS624 activity, although the later has not been reported previously. Endotoxin tests, shown in Supplementary Fig. 8, reveal the presence of low levels of endotoxin in the EPS624, chitosan and alginate used. EPS624 has the highest level, followed by chitosan and alginate, however all concentrations are below 0.5EU/mL, regarded as an acceptable range by the FDA for implantation of human medical devices in contact with the cardiovascular or lymphatic system [52]. Therefore, it seems unlikely that endotoxin is a major contributing factor to the observed TNF-α secretion. A more plausible hypothesis is that the TNF-α secretion occurs due to the chitosan as the chitosan/alginate coating present the highest TNF-α secretion, and the residual bacterial contaminants in EPS624. Improvements could be made in the EPS624 production methods to further lower endotoxin and other contaminant levels, such as switching from a broth to agar bacteria seeding to a glycerol stock to agar seeding, which could reduce the quantity of potential contaminants contained in the broth to be purified later in the process. A chitosan with a different molecular weight could also be an alternative to further modulate the TNF-α response and subsequent biological response. For example, TNF-α at 5ng/mL combined with EPS624 was found to prevent osteoclasts differentiation and activation [16]. Additional in vivo experiments are required to demonstrate the functionality of the EPS624/chitosan coatings.

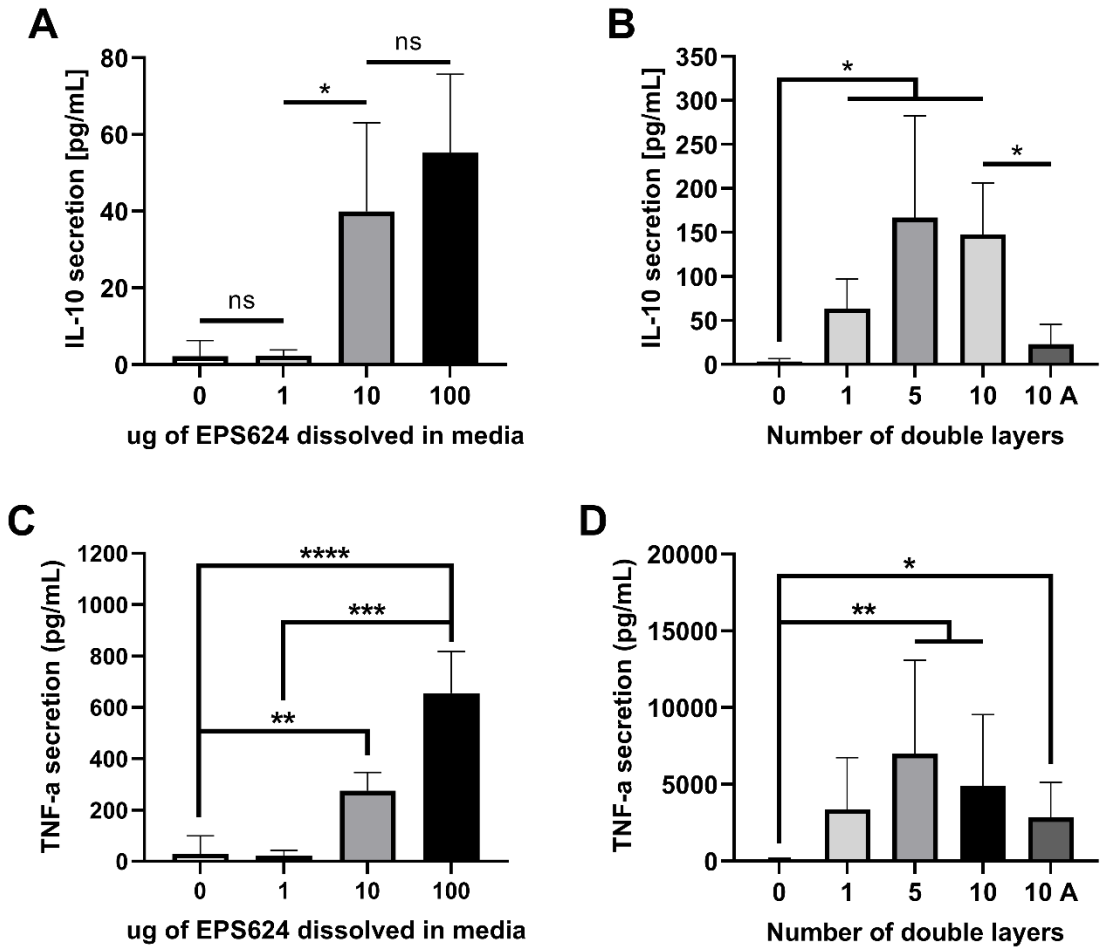

Figure 11: A: human peripheral blood mononuclear cells secretion of IL-10 when exposed to EPS624 dissolved in media at various concentrations for 24h, quantified by U-plex measurement; B: human peripheral blood mononuclear cells secretion of IL-10 when exposed to EPS624/chitosan with different number of layers or alginate/chitosan with 10 layers (10A) polyelectrolyte coatings for 24h , quantified by U-plex measurement; C: human peripheral blood mononuclear cells secretion of TNF- α when exposed to EPS624 dissolved in media at various concentrations for 24h, quantified by U-plex measurement; D: human peripheral blood mononuclear cells secretion of TNF-α when exposed to EPS624/chitosan with different number of layers or alginate/chitosan with 10 layers (10A) polyelectrolyte coatings for 24h, quantified by U-plex measurement. For both TNF-α and IL-10 measurement, for each group N=3 (each point being the average of an experiment), each experiment has n=3 for each condition

Conclusion:

In this work polyelectrolyte multilayer coatings based on EPS624 and chitosan were successfully developed. The polyelectrolyte films showed an exponential growth with increased topography and rugosity. The coatings effectively stimulated a specific IL-10 secretion by hPBMCs reaching concentrations equivalent or higher to concentrations measured in presence of EPS624 solubilized in media. Additionally, the coatings remained functional for at least 7 days, inducing a significant IL-10

secretion. Pending further purification of the materials used, these coatings hold potential in instructing pro-healing inflammatory conditions for local immunomodulatory applications.

Acknowledgements

We acknowledge Pamela Furlong for her help in the acquisition of the Scanning Electron Microscopy images. We acknowledge Adeline Tronel for her help in Zeta Potential and Dynamic Light Scattering measurements collection.

Funding

This work was funded by AO Trauma, grant number AR2018_04.

(1) Limoli, D. H.; Jones, C. J.; Wozniak, D. J. Bacterial Extracellular Polysaccharides in Biofilm Formation and Function. *Microbiol Spectr* **2015**, *3* (3). DOI: 10.1128/microbiolspec.MB-0011-2014.
(2) Freitas, F.; Torres, C. A. V.; Reis, M. A. M. Engineering aspects of microbial exopolysaccharide production. *Bioresour Technol* **2017**, *245* (Pt B), 1674-1683. DOI: 10.1016/j.biortech.2017.05.092.
(3) Klaus W. E. Rudolph, M. G., Firous Ebrahim-Nesbat, Matthias Nöllenburg, Alim Zomorodian, Kerstin Wydra, Michael Neugebauer, Ursula Hettwer, Wagih El-Shouny, Bernd Sonnenberg & Zoltan Klement the role of extracellular polysaccharides as virulence factors for phytopathogenic pseudomonads and xanthomonads. *Molecular mechanisms of bacterial virulence* **1994**, 357-378.
(4) Castro-Bravo, N.; Wells, J. M.; Margolles, A.; Ruas-Madiedo, P. Interactions of Surface Exopolysaccharides From Bifidobacterium and Lactobacillus Within the Intestinal Environment. *Front Microbiol* **2018**, *9*, 2426. DOI: 10.3389/fmicb.2018.02426.
(5) Qiu, Y.; Qiu, L.; Cui, J.; Wei, Q. Bacterial cellulose and bacterial cellulose-vaccarin membranes for wound healing. *Mater Sci Eng C Mater Biol Appl* **2016**, *59*, 303-309. DOI: 10.1016/j.msec.2015.10.016.
(6) Pourali, P.; Yahyaei, B. Wound healing property of a gel prepared by the combination of Pseudomonas aeruginosa alginate and Alhagi maurorum aqueous extract in rats. *Dermatol Ther* **2019**, *32* (1), e12779. DOI: 10.1111/dth.12779.
(7) Kumar, A.; Rao, K. M.; Han, S. S. Application of xanthan gum as polysaccharide in tissue engineering: A review. *Carbohydr Polym* **2018**, *180*, 128-144. DOI: 10.1016/j.carbpol.2017.10.009.
(8) Bagnol, R.; Grijpma, D.; Eglin, D.; Moriarty, T. F. The production and application of bacterial exopolysaccharides as biomaterials for bone regeneration. *Carbohydr Polym* **2022**, *291*, 119550. DOI: 10.1016/j.carbpol.2022.119550.
(9) Mohd Nadzir, M.; Nurhayati, R. W.; Idris, F. N.; Nguyen, M. H. Biomedical Applications of Bacterial Exopolysaccharides: A Review. *Polymers (Basel)* **2021**, *13* (4). DOI: 10.3390/polym13040530.
(10) Vidhyalakshmi, R.; Valli, N. C.; Narendra Kumar, G.; Sunkar, S. Bacillus circulans exopolysaccharide: Production, characterization and bioactivities. *Int J Biol Macromol* **2016**, *87*, 405-414. DOI: 10.1016/j.ijbiomac.2016.02.001.
(11) El-Newary, S. A.; Ibrahim, A. Y.; Asker, M. S.; Mahmoud, M. G.; El Awady, M. E. Production, characterization and biological activities of acidic exopolysaccharide from marine Bacillus amyloliquefaciens 3MS 2017. *Asian Pac J Trop Med* **2017**, *10* (7), 652-662. DOI: 10.1016/j.apjtm.2017.07.005.
(12) Dinic, M.; Pecikoza, U.; Djokic, J.; Stepanovic-Petrovic, R.; Milenkovic, M.; Stevanovic, M.; Filipovic, N.; Begovic, J.; Golic, N.; Lukic, J. Exopolysaccharide Produced by Probiotic Strain Lactobacillus paraplantarum BGCG11 Reduces Inflammatory Hyperalgesia in Rats. *Front Pharmacol* **2018**, *9*, 1. DOI: 10.3389/fphar.2018.00001.

(13) Altmann, F.; Kosma, P.; O'Callaghan, A.; Leahy, S.; Bottacini, F.; Molloy, E.; Plattner, S.; Schiavi, E.; Gleinser, M.; Groeger, D.; et al. Genome Analysis and Characterisation of the Exopolysaccharide Produced by Bifidobacterium longum subsp. longum 35624. *PLoS One* **2016**, *11* (9), e0162983. DOI: 10.1371/journal.pone.0162983.
(14) Schiavi, E.; Gleinser, M.; Molloy, E.; Groeger, D.; Frei, R.; Ferstl, R.; Rodriguez-Perez, N.; Ziegler, M.; Grant, R.; Moriarty, T. F.; et al. The Surface-Associated Exopolysaccharide of Bifidobacterium longum 35624 Plays an Essential Role in Dampening Host Proinflammatory Responses and Repressing Local TH17 Responses. *Appl Environ Microbiol* **2016**, *82* (24), 7185-7196. DOI: 10.1128/AEM.02238-16.
(15) Schiavi, E.; Plattner, S.; Rodriguez-Perez, N.; Barcik, W.; Frei, R.; Ferstl, R.; Kurnik-Lucka, M.; Groeger, D.; Grant, R.; Roper, J.; et al. Exopolysaccharide from Bifidobacterium longum subsp. longum 35624 modulates murine allergic airway responses. *Benef Microbes* **2018**, *9* (5), 761-773. DOI: 10.3920/BM2017.0180.
(16) Wallimann, A.; Hildebrand, M.; Groeger, D.; Stanic, B.; Akdis, C. A.; Zeiter, S.; Richards, R. G.; Moriarty, T. F.; O'Mahony, L.; Thompson, K. An Exopolysaccharide Produced by Bifidobacterium longum 35624(R) Inhibits Osteoclast Formation via a TLR2-Dependent Mechanism. *Calcif Tissue Int* **2021**, *108* (5), 654-666. DOI: 10.1007/s00223-020-00790-4.
(17) Boudou, T.; Crouzier, T.; Ren, K.; Blin, G.; Picart, C. Multiple functionalities of polyelectrolyte multilayer films: new biomedical applications. *Adv Mater* **2010**, *22* (4), 441-467. DOI: 10.1002/adma.200901327.
(18) Cai, K.; Rechtenbach, A.; Hao, J.; Bossert, J.; Jandt, K. D. Polysaccharide-protein surface modification of titanium via a layer-by-layer technique: characterization and cell behaviour aspects. *Biomaterials* **2005**, *26* (30), 5960-5971. DOI: 10.1016/j.biomaterials.2005.03.020.
(19) Serizawa, T.; Yamaguchi, M.; Akashi, M. Alternating bioactivity of polymeric layer-by-layer assemblies: anticoagulation vs procoagulation of human blood. *Biomacromolecules* **2002**, *3* (4), 724-731. DOI: 10.1021/bm0200027. Meng, S.; Liu, Z.; Shen, L.; Guo, Z.; Chou, L. L.; Zhong, W.; Du, Q.; Ge, J. The effect of a layer-by-layer chitosan-heparin coating on the endothelialization and coagulation properties of a coronary stent system. *Biomaterials* **2009**, *30* (12), 2276-2283. DOI: 10.1016/j.biomaterials.2008.12.075.
(20) Yao Shu, G. O., 2 Li Wang,3 Jingcai Zou,1 and Quanli Li4. Surface Modification of Titanium with Heparin-Chitosan Multilayers via Layer-by-Layer Self-Assembly Technique. *Journal of Nanomaterials* **2010**, *Volue 2011*. DOI: doi:10.1155/2011/423686.
(21) Fu, J.; Ji, J.; Yuan, W.; Shen, J. Construction of anti-adhesive and antibacterial multilayer films via layer-by-layer assembly of heparin and chitosan. *Biomaterials* **2005**, *26* (33), 6684-6692. DOI: 10.1016/j.biomaterials.2005.04.034.
(22) Angela Mutschler, ‡ Lorene Tallet,` †,‡ Morgane Rabineau,†,‡ Camille Dollinger,†,§; Marie-Helé ne Metz-Boutigue, ‡ Francis Schneider,†,∥ Bernard Senger,†,‡ Nihal Engin Vrana,†,§; Pierre Schaaf, ‡,⊥ and Philippe Lavalle*,†,‡. Unexpected Bactericidal Activity of Poly(arginine)/Hyaluronan Nanolayered Coatings. *Chem. Mater.* **2016**, *28*, 8700-8709.
(23) Antmen, E.; Muller, C. B.; Calligaro, C.; Dupret-Bories, A.; Barthes, J.; Lavalle, P.; Vrana, N. E. In vitro two-step granuloma formation model for testing innate immune response to implants and coatings. *Biomater Adv* **2022**, *138*, 212872. DOI: 10.1016/j.bioadv.2022.212872.
(24) Liam O'Mahony, S. P., Friedrich Altmann, Paul Kosma. USE OF BIFIDOBACTERIUM LONGUM AND AN EXOPOLYSACCHARIDE PRODUCED THEREBY. US 2018.
(25) Yan, Y.; Chang, S.; Wang, T.; Geng, Y. Scratch on Polymer Materials Using AFM Tip-Based Approach: A Review. *Polymers (Basel)* **2019**, *11* (10). DOI: 10.3390/polym11101590.
(26) J.L. Hutter, J. B. Calibration of atomic-force microscope tip. *Rev. Sci. Instrum.* **1993**, *64*, 1868-1873.
(27) Meredith, D. O.; Eschbach, L.; Wood, M. A.; Riehle, M. O.; Curtis, A. S. G.; Richards, R. G. Human fibroblast reactions to standard and electropolished titanium and Ti-6Al-7Nb, and electropolished stainless steel. *Journal of Biomedical Materials Research Part A* **2005**, *75a* (3), 541-555. DOI: 10.1002/jbm.a.30457.
(28) Nwodo, U. U.; Green, E.; Okoh, A. I. Bacterial exopolysaccharides: functionality and prospects. *Int J Mol Sci* **2012**, *13* (11), 14002-14015. DOI: 10.3390/ijms131114002.

(29) Swain, S. K.; Dey, R. K.; Islam, M.; Patel, R. K.; Jha, U.; Patnaik, T.; Airoldi, C. Removal of Fluoride from Aqueous Solution Using Aluminum-Impregnated Chitosan Biopolymer. *Sep Sci Technol* **2009**, *44* (9), 2096-2116. DOI: 10.1080/01496390902881212. Aïder, N. S. M. Zeta Potential and Turbidimetry Analyzes for the Evaluation of Chitosan/Phytic Acid Complex Formation. *Journal of Food Research* **2014**, *3*. DOI: doi:10.5539/jfr.v3n2p71.
(30) B. Maciel, C. O., N. Willenbacher Chain flexibility and dynamics of alginate solutions in different solvents. *Colloid and Polymer Science* **2020**, *298*, 791–801.
(31) Caridade, S. G.; Monge, C.; Almodovar, J.; Guillot, R.; Lavaud, J.; Josserand, V.; Coll, J. L.; Mano, J. F.; Picart, C. Myoconductive and osteoinductive free-standing polysaccharide membranes. *Acta Biomater* **2015**, *15*, 139-149. DOI: 10.1016/j.actbio.2014.12.027. Schneider, A.; Richert, L.; Francius, G.; Voegel, J. C.; Picart, C. Elasticity, biodegradability and cell adhesive properties of chitosan/hyaluronan multilayer films. *Biomed Mater* **2007**, *2* (1), S45-51. DOI: 10.1088/1748-6041/2/1/S07.
(32) Seon, L.; Parat, A.; Gaudiere, F.; Voegel, J. C.; Auzely-Velty, R.; Lorchat, P.; Coche-Guerente, L.; Senger, B.; Schaaf, P.; Jierry, L.; et al. Influence of the interaction strength between supramolecular complexes on the topography of neutral polymer multilayer films. *Langmuir* **2014**, *30* (22), 6479-6488. DOI: 10.1021/la501403m.
(33) Boddohi, S.; Killingsworth, C. E.; Kipper, M. J. Polyelectrolyte multilayer assembly as a function of pH and ionic strength using the polysaccharides chitosan and heparin. *Biomacromolecules* **2008**, *9* (7), 2021-2028. DOI: 10.1021/bm8002573.
(34) Picart, C.; Mutterer, J.; Richert, L.; Luo, Y.; Prestwich, G. D.; Schaaf, P.; Voegel, J. C.; Lavalle, P. Molecular basis for the explanation of the exponential growth of polyelectrolyte multilayers. *Proc Natl Acad Sci U S A* **2002**, *99* (20), 12531-12535. DOI: 10.1073/pnas.202486099.
(35) Almodovar, J.; Place, L. W.; Gogolski, J.; Erickson, K.; Kipper, M. J. Layer-by-layer assembly of polysaccharide-based polyelectrolyte multilayers: a spectroscopic study of hydrophilicity, composition, and ion pairing. *Biomacromolecules* **2011**, *12* (7), 2755-2765. DOI: 10.1021/bm200519y.
(36) Crouzier, T.; Picart, C. Ion pairing and hydration in polyelectrolyte multilayer films containing polysaccharides. *Biomacromolecules* **2009**, *10* (2), 433-442. DOI: 10.1021/bm8012378.
(37) Zhang, W.; Yang, Y.; Cui, B. New perspectives on the roles of nanoscale surface topography in modulating intracellular signaling. *Curr Opin Solid State Mater Sci* **2021**, *25* (1). DOI: 10.1016/j.cossms.2020.100873.
(38) Wells, R. G. The role of matrix stiffness in regulating cell behavior. *Hepatology* **2008**, *47* (4), 1394-1400. DOI: 10.1002/hep.22193.
(39) Liu, L. Y.; Chen, X. D.; Wu, B. Y.; Jiang, Q. [Influence of Aloe polysaccharide on proliferation and hyaluronic acid and hydroxyproline secretion of human fibroblasts in vitro]. *Zhong Xi Yi Jie He Xue Bao* **2010**, *8* (3), 256-262. DOI: 10.3736/jcim20100310.
(40) Sahana, T. G.; Rekha, P. D. A bioactive exopolysaccharide from marine bacteria Alteromonas sp. PRIM-28 and its role in cell proliferation and wound healing in vitro. *Int J Biol Macromol* **2019**, *131*, 10-18. DOI: 10.1016/j.ijbiomac.2019.03.048.
(41) Tran, P. A.; Webster, T. J. Understanding the wetting properties of nanostructured selenium coatings: the role of nanostructured surface roughness and air-pocket formation. *Int J Nanomedicine* **2013**, *8*, 2001-2009. DOI: 10.2147/IJN.S42970.
(42) Harvey, A. G.; Hill, E. W.; Bayat, A. Designing implant surface topography for improved biocompatibility. *Expert Rev Med Devices* **2013**, *10* (2), 257-267. DOI: 10.1586/erd.12.82.
(43) Lampin, M.; Warocquier, C.; Legris, C.; Degrange, M.; Sigot-Luizard, M. F. Correlation between substratum roughness and wettability, cell adhesion, and cell migration. *J Biomed Mater Res* **1997**, *36* (1), 99-108. DOI: 10.1002/(sici)1097-4636(199707)36:1<99::aid-jbm12>3.0.co;2-e.
(44) Tamada, Y.; Ikada, Y. Fibroblast growth on polymer surfaces and biosynthesis of collagen. *J Biomed Mater Res* **1994**, *28* (7), 783-789. DOI: 10.1002/jbm.820280705. Kang, I. K.; Ito, Y.; Sisido, M.; Imanishi, Y. Attachment and growth of fibroblast cells on polypeptide derivatives. *J Biomed Mater Res* **1989**, *23* (2), 223-239. DOI: 10.1002/jbm.820230207.

(45) den Braber, E. T.; de Ruijter, J. E.; Ginsel, L. A.; von Recum, A. F.; Jansen, J. A. Orientation of ECM protein deposition, fibroblast cytoskeleton, and attachment complex components on silicone microgrooved surfaces. *J Biomed Mater Res* **1998**, *40* (2), 291-300. DOI: 10.1002/(sici)1097-4636(199805)40:2<291::aid-jbm14>3.0.co;2-p. Uttayarat, P.; Toworfe, G. K.; Dietrich, F.; Lelkes, P. I.; Composto, R. J. Topographic guidance of endothelial cells on silicone surfaces with micro- to nanogrooves: orientation of actin filaments and focal adhesions. *J Biomed Mater Res A* **2005**, *75* (3), 668-680. DOI: 10.1002/jbm.a.30478. Oakley, C.; Brunette, D. M. The sequence of alignment of microtubules, focal contacts and actin filaments in fibroblasts spreading on smooth and grooved titanium substrata. *J Cell Sci* **1993**, *106 (Pt 1)*, 343-354. DOI: 10.1242/jcs.106.1.343.
(46) Chou, S. Y.; Cheng, C. M.; LeDuc, P. R. Composite polymer systems with control of local substrate elasticity and their effect on cytoskeletal and morphological characteristics of adherent cells. *Biomaterials* **2009**, *30* (18), 3136-3142. DOI: 10.1016/j.biomaterials.2009.02.037. Engler, A.; Bacakova, L.; Newman, C.; Hategan, A.; Griffin, M.; Discher, D. Substrate compliance versus ligand density in cell on gel responses. *Biophys J* **2004**, *86* (1 Pt 1), 617-628. DOI: 10.1016/S0006-3495(04)74140-5.
(47) Tan, L.; Fu, J.; Feng, F.; Liu, X.; Cui, Z.; Li, B.; Han, Y.; Zheng, Y.; Yeung, K. W. K.; Li, Z.; et al. Engineered probiotics biofilm enhances osseointegration via immunoregulation and anti-infection. *Sci Adv* **2020**, *6* (46). DOI: 10.1126/sciadv.aba5723.
(48) Davison, N. L., Barrère-de Groot, F., & Grijpma, D. W. . *Degradation of Biomaterials.*; 2014.
(49) Vasconcelos, D. P.; Costa, M.; Amaral, I. F.; Barbosa, M. A.; Aguas, A. P.; Barbosa, J. N. Modulation of the inflammatory response to chitosan through M2 macrophage polarization using pro-resolution mediators. *Biomaterials* **2015**, *37*, 116-123. DOI: 10.1016/j.biomaterials.2014.10.035. Huang, Y. C.; Vieira, A.; Huang, K. L.; Yeh, M. K.; Chiang, C. H. Pulmonary inflammation caused by chitosan microparticles. *J Biomed Mater Res A* **2005**, *75* (2), 283-287. DOI: 10.1002/jbm.a.30421.
(50) Fong, D.; Hoemann, C. D. Chitosan immunomodulatory properties: perspectives on the impact of structural properties and dosage. *Future Sci OA* **2018**, *4* (1), FSO225. DOI: 10.4155/fsoa-2017-0064.
(51) Ribeiro, J. C. V.; Forte, T. C. M.; Tavares, S. J. S.; Andrade, F. K.; Vieira, R. S.; Lima, V. The effects of the molecular weight of chitosan on the tissue inflammatory response. *J Biomed Mater Res A* **2021**, *109* (12), 2556-2569. DOI: 10.1002/jbm.a.37250.
(52) *Guidance for Industry: Pyrogen and Endotoxins Testing: Questions and Answers*. 2012. https://www.fda.gov/regulatory-information/search-fda-guidance-documents/guidance-industry-pyrogen-and-endotoxins-testing-questions-and-answers#:~:text=What%20are%20the%20endotoxins%20limits%20for%20medical%20devices%3F,-The%20Center%20for&text=For%20medical%20devices%2C%20using%20the,cardiovascular%20system%20and%20lymphatic%20system. (accessed.